POLITECNICO DI TORINO
Repository ISTITUZIONALE

Study of Polyelectrolyte/Silica Coatings Based on Layer-by-Layer Assembly on Iron Powder for Soft Magnetic Composite Materials

Original
Study of Polyelectrolyte/Silica Coatings Based on Layer-by-Layer Assembly on Iron Powder for Soft Magnetic Composite Materials / Poškovi, E., Noro, L., Abba, L., Franchini, F., Minervini, M., Ferraris, L., Carosio, F., Actis Grande, M., Tenconi, A.. - In: COATINGS. - ISSN 2079-6412. - ELETTRONICO. - 16:10(2026), pp. 1-16. [10.3390/coatings16101148]

Availability:
This version is available at: 11583/3016075 since: 2026-09-29T15:11:11Z

Publisher:
MDPI

Published
DOI:10.3390/coatings16101148

Terms of use:

This article is made available under terms and conditions as specified in the corresponding bibliographic description in the repository

Publisher copyright

(Article begins on next page)

12 November 2026

coatings

MDPI

Article

Study of Polyelectrolyte/Silica Coatings Based on Layer-by-Layer Assembly on Iron Powder for Soft Magnetic Composite Materials

Emir Pošković [1,*], Luca Noro [1], Lorenza Abbà [2], Fausto Franchini [1], Marcello Minervini [3], Luca Ferraris [1], Federico Carosio [2], Marco Actis Grande [2] and Alberto Tenconi [1]

[1] Department of Energy "Galileo Ferraris", Politecnico di Torino, 10129 Torino, Italy; luca.noro@polito.it (L.N.); fausto.franchini@polito.it (F.F.); luca.ferraris@polito.it (L.F.); alberto.tenconi@polito.it (A.T.)
[2] Department of Applied Science and Technology, Politecnico di Torino, 10129 Torino, Italy; lorenza.abba@polito.it (L.A.); federico.carosio@polito.it (F.C.); marco.actis@polito.it (M.A.G.)
[3] Department of Engineering and Applied Sciences, University of Bergamo, 24129 Bergamo, Italy; marcello.minervini@unibg.it
* Correspondence: emir.poskovic@polito.it

Highlights

What are the main findings?

- The final SMC properties can be tuned with the LbL process reagent concentration.
- The final magnetic permeability can be improved with a sufficient barrier against oxidation.

What are the implications of the main findings?

- The layer-by-layer process allows the fabrication of effective insulating/binding layers for SMCs
- Silica nanoparticle suspensions can create a barrier against the oxidation of the iron substrate.

Abstract

Soft Magnetic Composites (SMCs)—powdered ferromagnetic materials characterized by high macroscopic electrical resistivity—constitute an excellent resource for electrical machines with non-traditional magnetic flux configurations, such as axial flux machines. Their adoption is currently expanding within the mass production of small components, particularly in the automotive sector. Consequently, numerous research activities focus on performance optimization to maximize and harmonize the mechanical, energetic, and magnetic properties of SMCs. In this context, the layer-by-layer (LbL) chemical deposition process offers multiple degrees of freedom regarding the types, quantities, and arrangements of materials used to construct insulating and binding layers. This study presents a specific system comprising a polymer and nanometric silica, investigating the influence of several process parameters on the overall performance of the final material. The resulting samples were characterized using a hysteresigraph to determine their magnetization curves, relative magnetic permeability, and specific losses across different frequencies. Additionally, mechanical properties were evaluated through transverse rupture strength tests.

Keywords: magnetic materials; electrical machines; layer-by-layer; soft magnetic composites

Check for updates

Academic Editor: Gianni Barucca

Received: 4 August 2026
Revised: 12 September 2026
Accepted: 21 September 2026
Published: 26 September 2026

Copyright: © 2026 by the authors. Licensee MDPI, Basel, Switzerland. This article is an open access article distributed under the terms and conditions of the Creative Commons Attribution (CC BY) license.

1. Introduction

Advanced energy management that improves efficiency while preserving the environment has become a critical focus in recent research [1–5]. In this context, several materials

play a major role, including magnets [6–9]. Magnets are broadly divided into hard and soft categories. Innovation in hard magnetic materials focuses on rare-earth-free solutions based on new alloys or recycled materials [10–15]. Conversely, for soft magnetic materials, the development path depends closely on the specific application [16,17]; however, to maximize energy efficiency, the choice typically lies between additive manufacturing magnetic materials and soft magnetic composite materials [18–20].

Soft Magnetic Composites (SMCs) are promising materials made of compacted ferromagnetic powders whose grains are electrically insulated from each other by means of thin coating layers. Their main advantage is a dramatic reduction in eddy current losses compared to bulk materials; as a result, within a specific frequency range, the hysteresis loop maintains almost the same shape and width. However, this property is achieved at the cost of a significant reduction in mechanical performance compared to magnetic sheets, as well as a higher coercivity, which leads to greater losses at low frequencies. The nature and functionality of the insulating layer play a key role in the final material properties. To avoid degrading the relative magnetic permeability, the weight percentage of the layer material must be kept to a minimum. Conversely, ensuring effective electrical insulation between grains requires sufficient spacing, meaning that the thickness of the coating cannot fall below a minimum value. Since the layer material also acts as a binder, it strongly influences the macroscopic mechanical properties. Consequently, a wide variety of technologies and processes are available for layer fabrication, each offering distinct advantages and challenges [21].

The most common insulating layer is produced by phosphating and coating ferromagnetic powder with phosphoric acid [22–24]. The obtained layer is inorganic, offering excellent energetic performance but moderate magnetic properties. Another solution involves using an organic layer, typically based on epoxy resins and occasionally phenolic binders [25–27]. The simplicity and versatility of polymer techniques, combined with a well-balanced mix of magnetic, energetic, and mechanical properties, render organic-layered SMCs a promising choice for specific static applications, such as in the telecommunications sector. However, their lower resistance to the thermal treatment required for relieving residual mechanical stress after compaction limits the widespread use of these organic SMCs. Alternatively, other inorganic SMCs employ metal oxides as insulating layers, most notably various types of ferrites and silica. Ferrite layers are prepared using different techniques [28–32], and can also exhibit magnetic behavior. Their primary drawback relates to poor mechanical properties. For silica layers, several coating processes have recently been investigated [33–38], particularly due to their high electrical resistivity. Although they offer some advantages, the difficulty of controlling the coating process and their inferior mechanical properties hinder their widespread adoption. Other metal oxides, such as aluminum oxide [39,40], provide distinct benefits; however, the high oxidation state of the ferromagnetic material limits their application. Therefore, achieving an optimal insulating layer likely requires a combination of inorganic and organic materials to balance the whole set of characteristics.

The present work focuses on a specific family of systems fabricated via the layer-by-layer chemical deposition process [41,42]. This technique enables the growth of nanometric layer stacks composed of both organic and inorganic materials; its application in SMC processing provides numerous degrees of freedom regarding the nature, thickness, quantity, and arrangement of the layers.

The systems investigated herein consist of three or five layers containing branched polyethylenimine (BPEI) as the positively charged solution, and polyacrylic acid (PAA) and silica as the negatively charged dispersion. Consequently, this architecture can be

classified as a hybrid system, leveraging both inorganic and organic materials to construct an insulating coating.

The primary objective of this study is to investigate how the silica weight percentage and the number of layers influence the resulting magnetic, energetic, and mechanical properties.

2. Materials and Methods

2.1. Materials

The base powder used in all systems investigated in the present work is FeABC 100.30, supplied by Höganäs AB (Höganäs, Sweden). This water-atomized iron powder exhibits a particle size distribution ranging from 45 to 250 µm and a purity greater than 99.95%. Branched polyethylenimine (BPEI, weight-average molecular weight Mw ~ 25,000 Da by light scattering, number-average molecular weight Mn ~ 10,000 by gel permeation chromatography, according to the material data sheet), polyacrylic acid (PAA, average Mw ~ 250,000, 35 wt% in water), colloidal silica (LUDOX® TM-40, SiO_2, 40 wt% in water, produced by Grace, Columbia, MD, USA) and sodium hydroxide (NaOH) were purchased from Sigma Aldrich (Milwaukee, WI, USA). BPEI was dissolved in deionized (DI) water up to 1 wt% concentration. Colloidal silica was added, in different concentrations of 2 wt%, 4 wt% and 6 wt%, to a 1 wt% polyacrylic acid solution. All the solutions and dispersions were prepared using 18.2 MΩ·cm deionized water (which represents the standard purity grade typically employed for LbL assembly) supplied by a Q20 Millipore system (Milano, Italy) and kept under magnetic stirring overnight. The pH of the PAA + SiO_2 suspensions (monitored using a pH meter, edge series by HANNA, Woonsocket, RI, USA) was adjusted with NaOH 8 M to a pH of 9 in order to avoid powder oxidation.

The layer-by-layer deposition method relies on electrostatic interactions between reagents of opposite electrical polarities. The raw iron powder is immersed in the first solution for a specified duration and subsequently washed, resulting in the deposition of the first nanometric layer. The iron powder weight was 100 g, and the solution volume was 25 mL. This process is then repeated with the second solution to deposit a subsequent layer on top of the previous one. A polarity inversion occurs at each step: the previously deposited layer and the subsequent reagent, carrying opposite charges, exert a mutual attractive force that drives the formation of the new layer. The layer thickness can be controlled by tuning various parameters, including deposition time, reagent concentration, and solution pH. These immersion steps can be repeated to achieve the target number of layers. A scheme representing the process description steps is shown in Figure 1.

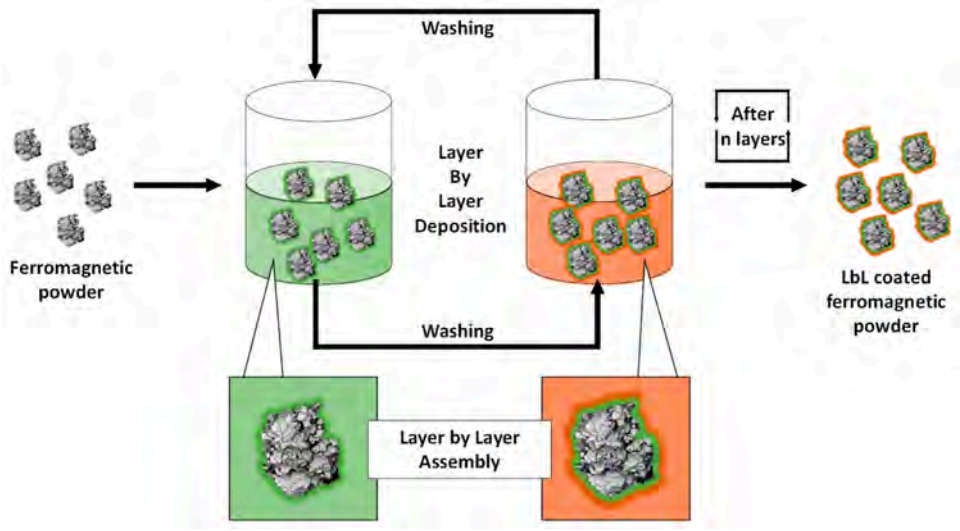

Figure 1. Layer-by-layer deposition process on iron powders.

In the implemented systems, the positive layers consist of branched polyethylenimine (BPEI), whereas the negative layers contain polyacrylic acid (PAA) and colloidal silica. The number of layers was also varied from 3 to 5, with both the first and last layers exhibiting positive polarity (polyethylenimine). The deposition time was fixed at 60 s, and after each deposition step, powders were washed with DI water.

Following the final washing step, all systems were dried in an oven at 80 °C in air for two hours.

Finally, the dried powder was cold-compacted at 800 MPa, as illustrated in Figure 2, in a die, and heat-treated at 180 °C in air for 1 h to form a rigid structure through the curing of PAA and to obtain the final soft magnetic composite (SMC) material, which exhibits enhanced magnetic properties and a high macroscopic electrical resistivity due to the combination of polymer–silica layers.

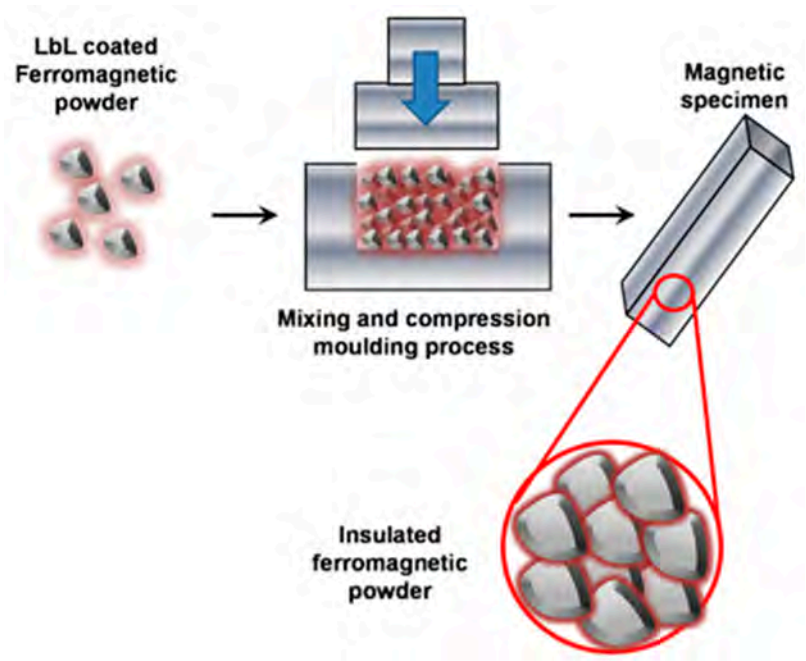

Figure 2. Compaction of the coated iron powder.

The electrical resistivity values of the samples in this study were not measured directly. The resistivity trend was qualitatively derived from high-frequency specific loss values, which are commonly correlated with macroscopic electrical resistivity.

2.2. Implemented Systems

The present work shows the results of six systems showing different coating process parameters varying the SiO_2 percentage content in the weight and the number of layers, which are modifications of the same system, as mentioned before; the system with 3 layers is indicated as 1.5 bilayers (1.5 BL), and the system with 5 layers is referred to as 2.5 bilayers (2.5 BL, as show in Table 1:

Table 1. Systems' composition summary.

Layer Number	Positive Layer	Negative Layer	SiO_2 wt%
3 (1.5 bilayers)	BPEI	PAA + SiO_2	2%
3 (1.5 bilayers)	BPEI	PAA + SiO_2	4%

Table 1. *Cont.*

Layer Number	Positive Layer	Negative Layer	SiO_2 wt%
3 (1.5 bilayers)	BPEI	PAA + SiO_2	6%
5 (2.5 bilayers)	BPEI	PAA + SiO_2	2%
5 (2.5 bilayers)	BPEI	PAA + SiO_2	4%
5 (2.5 bilayers)	BPEI	PAA + SiO_2	6%

The dried powders reported in Figure 3 were then compacted into thin bars using a double-punch molding machine. The final dimensions of the samples were approximately 55 mm × 10 mm × 3 mm. This particular shape meets the dimensional requirements of a custom-built single-sheet tester (SST), which was used for the magnetic characterization of the samples and can also be used to perform bending tests to obtain mechanical strength via a dynamometer.

Figure 3. Coated iron powder after the drying phase.

2.3. Coating Characterization

The growth of the LbL assembly was monitored on a model silicon wafer ((100), single polished) using a Fourier Transform Infrared (FT-IR) spectrophotometer (16 scans, 4 cm^{-1} resolution, Frontier, Perkin Elmer, Shelton, CT, USA) in transmission mode. The silicon wafer was dipped into the selected polyelectrolyte suspensions up to 2.5 BLs following the same procedure (in terms of deposition times and layer sequence) used to cover the iron powder. After each deposition step, the Si wafer was dried, and the IR spectrum of the deposited layer was collected.

Surface morphology, along with elemental analysis, of uncoated and LbL-coated iron powders was investigated using a ZEISS EVO 15 (Calr Zeiss Industrielle Messtechnik, Oberkochen, Germany) Scanning Electron Microscopy (SEM) and an energy-dispersive spectroscopy (EDS) probe of Oxford Ultim Max (Oxford Instruments, High Wycombe, UK).

2.4. Magnetic Characterization

The magnetic and energetic properties of the samples were measured at different frequencies from 10 Hz to 1000 Hz and up to 6500 A/m by means of a digitized waveforms hysteresigraph. Although the measurement method and the flux waveform control were compliant with the IEC 60404 standards (which generally refer to the magnetic materials' specifications and measurements, while Section 3 [43] relates to single-sheet testers and Section 6 [44] to AC test methods), the measurements obtained with the single-sheet tester are not fully compliant, since the standard states that the preferred shape is toroidal [45,46]. However, the results can be corrected by applying compensation factors previously determined by comparing thin bars measured with the SST against toroids made of the same material. The calibration factors were calculated by averaging the results of approximately ten datasets from various samples, which had been previously prepared and measured using both toroidal and thin bar geometries. Calibration involved adjusting two instrument parameters: the primary winding turn number (set to 94 instead of the actual value of 100) and the sample length (set to 37 mm instead of the nominal value of approximately 55 mm). This sample length compensation is applied exclusively within the induction calculation formulas, whereas the actual value is maintained for density calculations. This compensation method ensures high accuracy at low frequencies for all relevant magnetic and energy parameters.

The high-frequency response is also preserved by utilizing ferrite blocks instead of magnetic sheets for the closing yokes. The potential saturation of the ferrites is mitigated by employing blocks with a wide cross-section, ensuring that the entire yoke material remains far from saturation. The laboratory SST is shown in Figure 4.

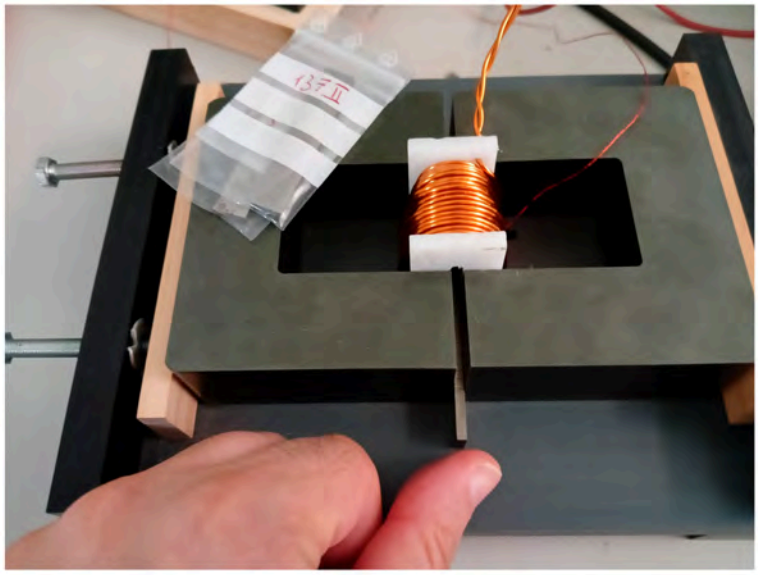

Figure 4. Singe-sheet tester with the BPEI/SiO_2 SMC samples under examination.

2.5. Mechanical Characterization

The mechanical properties are determined via the Transverse Rupture Strength (TRS) test, a bending test that measures the maximum mechanical strength of perpendicular specimens under a 3-point bending load. The force is recorded, and TRS is obtained using the standard formulation, accounting for the sample thickness and width. In Figure 5, the TRS test is shown after the sample is broken.

Tensile tests were performed by a Zwick-Roell machine (Zwick-Roell BT1-FR100, ZwickRoell GmbH & Co. KG, Ulm, Germany).

Figure 5. The TRS test with the BPEI/SiO_2 SMC sample under examination.

3. Results

3.1. Coating Growth on Model Substrate and Iron Powder

The LbL growth of the BPEI/[PAA + SiO_2] was studied up to 2.5 BLs by means of FT-IR spectroscopy on a model silicon substrate in order to evaluate the growth regime of the assembly (Figure 6).

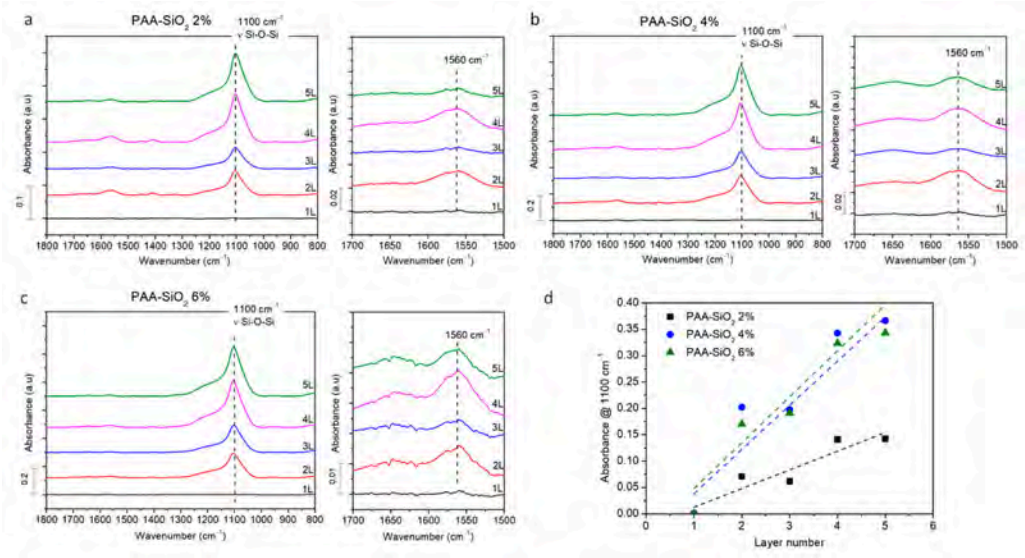

Figure 6. Coating growth on model silicon substrate: IR spectra at different deposited layers (plus additional magnified range graph) for PAA-SiO_2 2% (**a**), PAA-SiO_2 4% (**b**), PAA-SiO_2 6% (**c**) and absorbance of the signal at 1100 cm^{-1} vs. number of deposited layers (**d**).

The spectra of the single components, BPEI, PAA and SiO_2, are reported in Figure S1. BPEI shows a characteristic band at 1570 cm^{-1}, which is attributed to the NH_2 bending vibration and the asymmetric stretching of NH_3^+ groups, while the peak at 1475 cm^{-1} is associated with NH bending and the symmetric stretching of NH_3^+ [47]. The bands observed at 1410 and 1310 cm^{-1} are assigned to CH_2 deformation and twisting vibrations, respectively. In addition, C–N stretching vibrations can be identified in the 1180–1000 cm^{-1} region [48]. At basic pH, polyacrylic acid is almost fully deprotonated, with most of the

carboxylic acid groups converted into carboxylate ions (–COO^-). Consequently, the FT-IR spectrum shows the characteristic bands assigned to the asymmetric and symmetric stretching vibrations of the carboxylate groups, at 1560 cm^{-1} and 1450 cm^{-1} [49,50]. The IR spectrum of colloidal silica displays a main characteristic band at 1100 cm^{-1} related to Si-O-Si vibration [48,51].

When the components were LbL assembled on a silicon wafer, the main signal ascribed to colloidal silica (1100 cm^{-1} [52]) is clearly visible and grows proportionally with the number of PAA/SiO_2 layers deposited (Figure 6a–c). The presence of the two polyelectrolytes is highlighted by a band centered at 1560 cm^{-1}, likely resulting from the main signals of the PAA and BPEI functional groups.

By plotting the absorbance of the signal at 1100 cm^{-1} as a function of the number of layers deposited, a linear growth regime of the assembly is visible (Figure 6d). The absorbance of the assembly with 4 wt% silica is higher than that with 2 wt% silica. Different from what was expected, when the silica concentration is 6 wt%, no further increase in absorbance can be observed. This latter finding indicates that, with the adopted assembly conditions, the adsorption of silica during the deposition of the PAA/SiO_2 layer reaches saturation at 4 wt% SiO_2. Indeed, the adsorption of nanoparticles can display a saturation effect where similar layer growths are observed across different deposition times, thereby suggesting a threshold above which no further mass accumulation occurs [53].

The coatings were then transferred to iron powder depositing of either 1.5 or 2.5 BL (i.e., a total of 3 and 5 deposited layers). At such a low number of deposition steps, the coating produces minimal changes in particle morphology, rendering the particles only slightly smoother; Figure S2. The presence of the coating is highlighted by EDS analysis, which reveals the signal of Si with wt% below 0.5%, which corresponds to a total silica content of approximately 1%wt (Figures 7 and S3). This result is ascribed to the low number of deposited layers containing silica (i.e., one and two for 1.5 and 2.5 BL samples, respectively), thereby differing from conventional LbL coatings that typically incorporate 10–20 SiO_2 layers, inherently yielding higher Si concentration via EDS [54].

Moreover, the higher detection of carbon (C) compared to uncoated ferromagnetic particles could indicate the presence of a coating. Interestingly, coatings produced with 4 wt% and 6 wt% SiO_2 yielded similar results, thus confirming the behaviour observed on the model substrate.

At 5000× magnification, SEM images reveal differences between uncoated and coated ferromagnetic particles. The iron shows more regular surfaces, compared to the surface with softer lines for the proposed systems. Additionally, the iron surface shows very small points that are gradually covered as the silica percentage increases. Instead, the surfaces of 4 wt% and 6 wt% SiO_2 exhibit mossy deposits, confirming the presence of the coating.

3.2. Magnetic Properties

Hysteresigraph characterization at different frequencies is useful for separating iron losses into hysteresis losses (which approximately correspond to the iron losses at the lowest measured frequency) and dynamic losses (eddy current losses + excess losses). The maximum magnetic permeability and the induction value at 5000 A/m indicate the potential suitability of the material for static or rotating electrical machines. Depending on the final application, permeability values higher than 400 can be suitable for fabricating a stator iron core. The specific volumetric losses represent a normalization of the losses against the final density of the samples. Furthermore, the specific energy loss per loop provides a faster and more legible representation of the losses, enabling a clear comparison of different materials from an energetic perspective.

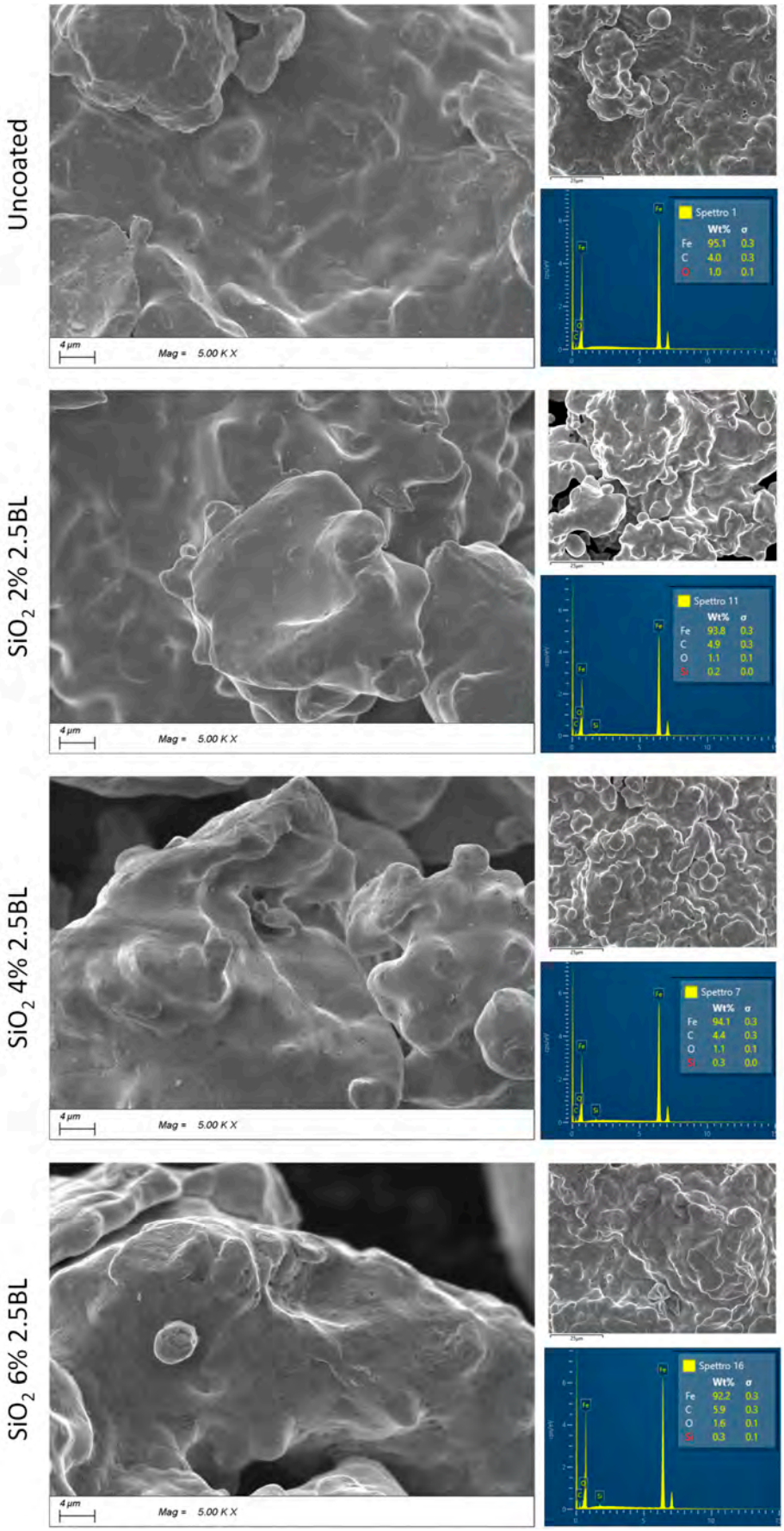

Figure 7. Microstructure analysis at 5000× and EDS measurements of uncoated and 2.5 BL (SiO_2 2%, 4% and 6%) coated iron powder.

Several phenomena and characteristics influence the material's final magnetic properties. The most important are the following:

- A greater amount of insulating material between the grains reduces the effective quantity of magnetically active material and lowers the mutual interaction between powder particles, resulting in reduced permeability and increased coercive field strength—and, consequently, increased specific losses;
- Degraded insulation—caused by non-uniform coating, potential rupture of the insulating layer during pressing, or non-negligible electrical conduction within the layer—does not affect magnetic and energy characteristics at lower frequencies (around 50 Hz); however, it negatively impacts specific losses at high frequencies, which increase exponentially with the material's volume conductivity;
- Surface oxidation of the particles can occur with low PH, leading to a significant, sometimes drastic, drop in permeability and a slight increase in coercive field strength.

A first comparison can involve the samples with a 3- and 5-layer deposition. Moreover, the SMC with the organic insulting layer, with very low epoxy resin content (0.2 wt%), prepared with traditional mixing and compacted at 800 MPa, is chosen as reference for comparison. In the following text, it is referred to as the Epoxy SMC reference. This SMC has a unique layer thicker than LbL nanolayers.

In Figure 8a,b, all proposed systems with 1.5 BL exhibit lower specific losses than the reference Epoxy SMC material. The lowest losses are obtained with SMC containing 4 wt% silica, and as the silica concentration increases, the iron losses increase. In addition, considering the density and volume, the lowest values are again obtained for 4 wt%, but other SMCs with SiO_2 are very close to the reference one (Figure 8b). Instead, in Figure 8c, the maximum magnetic permeability is obtained for the specimen with 2 wt% SiO_2 (443 @ 20 Hz), and the minimum is observed for 4 wt%. The reference is the second in order: that SMC with the lowest silica content has a layer thinner than the typical Epoxy SMC. The decrease in the maximum magnetic permeability in the considered frequency range is minimal for the system with 4% silica, which reaches 5.3%. The maximum reduction is observed for the Epoxy SMC reference and LbL SMC with 2 wt% of silica. The same behaviour is observed for magnetic induction at 5000 A/m (Figure 8d), with the maximum value observed for SMC with 2 wt% SiO_2 (1.42 T) and the minimum for 4 wt% (1.38). In Figure 8e, the lower trend in specific energy loss per loop is observed for SMC with 4 wt% SiO_2. In fact, the coefficient for hysteresis losses (y-intercept) is the second smallest for SMC with 4 wt% (the first is SMC with 2 wt%) and the lowest slope, which represents eddy current losses, is obtained for SMC with 4 wt%. Moreover, excess losses are observed for some proposed SMCs due to slight levelling in some trends, especially for the LbL SMC with a nanolayer with 4% silica. The lower dynamic losses confirm the lower magnetic permeability reduction in the considered frequency range.

The same behavior noted for LbL SMC 1.5 BL, related to the specific iron losses, is maintained for 2.5 BL, as shown in Figure 9a,b. Again, the lowest losses are observed with SMC containing 4 wt% silica. On the other hand, the magnetic permeability decreases across almost all systems relative to the Epoxy SMC reference (the maximum value is the same for the reference and the SMC with 2 wt% SiO_2), and the lowest value is obtained for the LbL SMC with 6 wt% SiO_2, as shown in Figure 9c. The minimum reduction for magnetic permeability is 5.1%, again observed for SMC with 4 wt% of silica. The lower reduction compared to 1.5 BL is due to the thicker insulating layer, which is able to better mitigate eddy currents. For magnetic induction of 5000 A/m, the behavior is very similar to that at the maximum magnetic permeability, only with a smaller difference between the values (Figure 9d). In the case of specific energy losses, the behavior is the same as in the case for 1.5 BL systems (Figure 9d).

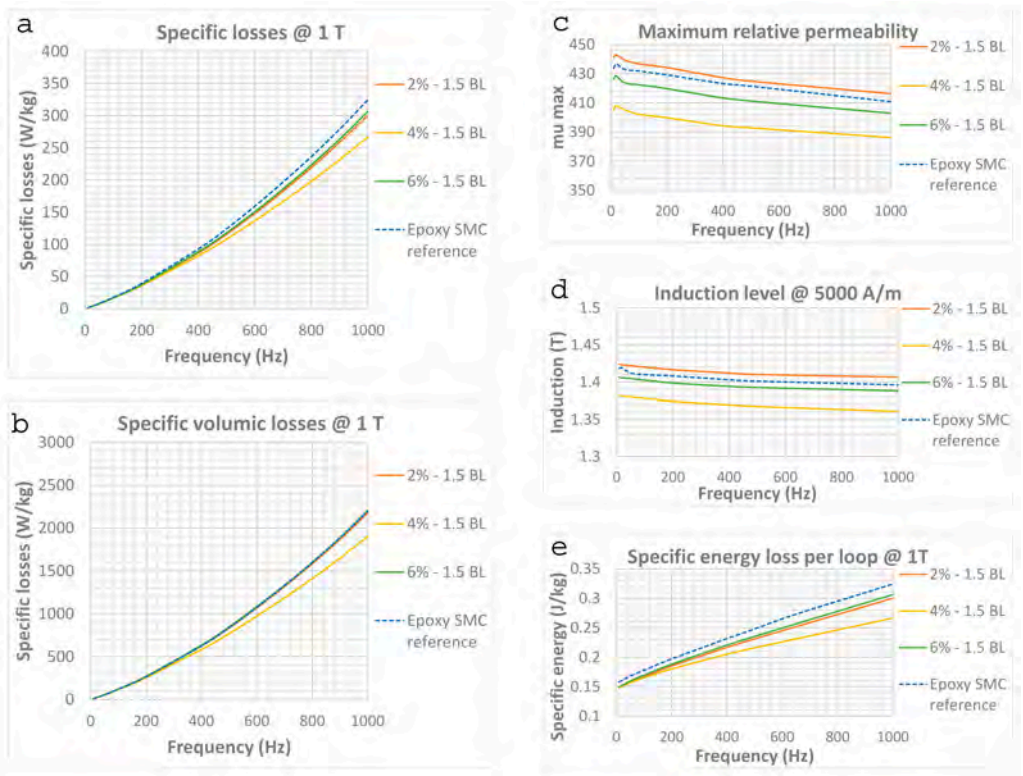

Figure 8. Magnetic and energetic comparison as a function of the variation in the SiO_2 with coating obtained with 1.5 BL (3 layers): Specific iron loss @1 T as a function of frequency related to weight (**a**) and volume (**b**); maximum relative magnetic permeability as a function of frequency (**c**); magnetic induction @ 5000 A/m as a function of frequency (**d**) and specific energy @ 1 T as a function of frequency (**e**).

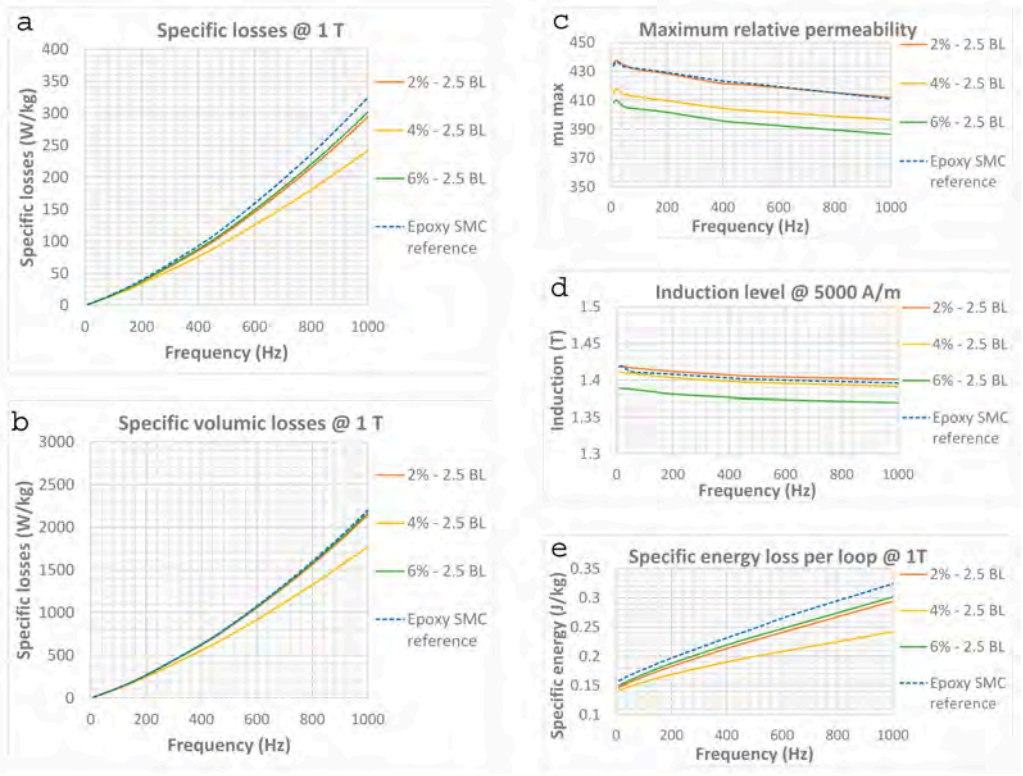

Figure 9. Magnetic and energetic comparison as a function of the variation in the SiO_2 with coating obtained with 2.5 BL (5 layers): Specific iron loss @1 T as a function of frequency related to weight (**a**) and volume (**b**); maximum relative magnetic permeability as a function of frequency (**c**); magnetic induction @ 5000 A/m as a function of frequency (**d**) and specific energy @ 1 T as a function of frequency (**e**).

3.3. Mechanical Properties

For mechanical properties (Figure 9), TRS and Young's modulus (Emod) are considered for a preliminary analysis; a reference SMC prepared with epoxy resin as binder is also reported in Table 2. The values obtained were also compared with those of the neat FeABC powder as supplied by the manufacturer, pressed under identical conditions, for which the TRS ranged from 25 to 32 MPa. This range is entirely consistent with the measurements presented here. Thus, by considering the mechanical properties of an epoxy-based SMC and the variability displayed by the neat uncoated powder, it can be inferred that coatings investigated in this study have no significant impact on the flexural mechanical properties of the compacted powder.

Table 2. Mechanical properties' summary.

Composition	Layer Num.	TRS	Young Modulus
		–/MPa	/GPa
2%	3	34.7	17.2
4%	3	26.8	15.8
6%	3	31.7	22.7
2%	5	30.9	20.7
4%	5	27.0	18.8
6%	5	35.9	22.6
Ref. Epoxy SMC	1	117.0	52.2

4. Discussion

A detailed comparison between the 1.5 BL and the 2.5 BL systems is discussed hereafter. From this point of view, some main values are reported in Table 3. The systems with 2.5 BL show lower permeability and, more or less, the same iron losses. Both systems containing 4 wt% of silica exhibit lower losses than the others, particularly at high frequencies. The systems with 2 wt% and 6 wt% silica show similar loss levels, regardless of the number of layers. Conversely, the two 4 wt% silica systems display slightly different losses depending on the layer count; specifically, the five-layer system exhibits lower high-frequency losses, suggesting enhanced insulation.

Table 3. Magnetic data summary: the blue values are the best for the considered parameters.

Composition	Layer Num.	Spec. Wt. Losses @50 Hz	Spec. Wt. Losses @400 Hz	Spec. Vol. Losses @50 Hz	Spec. Vol. Losses @400 Hz	Max Magnetic Permeability	B @ 5000 A/m	Density
		/W/kg	/W/kg	/W/dm^3	/W/dm^3	–	/T	/Kg/dm^3
2%	3	7.85	86.6	56.84	627	443	1.42	7.24
4%	3	7.82	82.0	55.81	585	408	1.38	7.13
6%	3	7.95	88.2	57.16	634	428	1.41	7.19
2%	5	7.76	85.4	56.52	621	437	1.42	7.28
4%	5	7.41	76.1	54.19	557	418	1.41	7.32
6%	5	7.94	87.7	56.98	629	410	1.39	7.17
Ref. Epoxy SMC	1	8.40	92.6	56.84	627	437	1.42	6.77

Regarding the five-layer systems, both the permeability and the induction at 5000 A/m follow a specific trend: the 2 wt% system exhibits the highest permeability, the 4 wt% system ranks intermediate, and the 6 wt% system shows the lowest. In contrast, the three-layer systems do not follow this trend for either permeability or induction at 5000 A/m; notably, the 4 wt% system exhibits the lowest value overall.

It can be hypothesized that a 4 wt% silica content promotes better particle insulation, thereby reducing high-frequency losses. This hypothesis is supported by the fact that the 4 wt% silica/five-layer configuration yields even lower high-frequency losses than the 4 wt%/three-layer counterpart, despite possessing higher permeability.

Moreover, the density data show high values for 4 wt and 2.5 BL. It is probably suggested that the coating with 4 wt% silica and five layers is very thin.

In summary, all details indicate that a silica concentration of 4% by weight represents an optimization of the deposition aspects that yield the greatest benefits for the magnetic and energetic properties of the final materials.

The comparison with reference SMC materials is almost always in favor, especially concerning energetic aspects. The lower density of the reference SMC is related to its 0.2 wt% epoxy resin content, indicating a very thick coating (even if the plastic content is very small), whereas LbL SMCs show a very thin covering.

5. Conclusions

In this work, it is demonstrated that efficient coating systems can be achieved via the layer-by-layer deposition technique with different layer numbers and silica concentrations for applications in soft magnetic materials for electrical machines. The hybrid coatings, based on the combination of the polymer BPEI and SiO_2 nanolayers, reduce eddy current losses and maintain good magnetic properties, especially at 4 wt% SiO_2. It is also demonstrated that increasing silica does not provide additional benefits. The comparison with reference SMC based on epoxy resin shows better energetic and magnetic properties, but lower mechanical resistance. The reason is that the epoxy resin, even in small quantities (0.2 wt%), is a layer thicker than LbL layers. From this point of view, the new layer combination will be investigated by adding other nanomaterials to improve mechanical properties or by adding epoxy resin to the last nanolayers at a content less than 0.1 wt%.

6. Patents

Processo per la produzione di materiali magnetici dolci nanorivestiti—Advanced Nano Insulated Magnetic Materials—Priority number: IT 102021000026681.

Supplementary Materials: The following supporting information can be downloaded at https://www.mdpi.com/article/10.3390/coatings16101148/s1, Figure S1: IR spectra of neat BPEI, pH9 PAA and SiO_2; Figure S2: SEM micrograph of uncoated and LbL-coated iron powder at magnification 1000×; Figure S3: Microstructure analysis at 5000× and EDS measurements of 1.5 BL coated iron powder.

Author Contributions: Conceptualization, E.P., F.F., L.F. and F.C.; methodology, E.P., L.N., F.F., M.M., L.F. and F.C.; software, E.P., L.N., L.A., and F.F.; validation, E.P., L.F., F.C. and M.A.G.; formal analysis, E.P., L.N., L.A., F.F., M.M. and F.C.; investigation, E.P., F.F., L.F. and F.C.; resources, E.P., L.F., F.C., M.A.G. and A.T.; data curation, E.P., L.N., L.A., F.F. and F.C.; writing—original draft preparation, E.P., L.A., F.F. and F.C.; writing—review and editing, E.P., L.F. and F.C.; visualization, E.P., L.F. and F.C.; supervision, L.F., F.C. and A.T. All authors have read and agreed to the published version of the manuscript.

Funding: This research received no external funding.

Institutional Review Board Statement: Not applicable.

Informed Consent Statement: Not applicable.

Data Availability Statement: The original contributions presented in this study are included in the article. Further inquiries can be directed to the corresponding author.

Conflicts of Interest: The authors declare no conflicts of interest.

Abbreviations

The following abbreviations are used in this manuscript:

SMC	Soft Magnetic Composite
LbL	Layer-by-Layer Deposition Process

References

1. Lepoutre, A.; Bouscayrol, A.; Irimia, C.; Husar, C.; Kalogiannis, T.; Ahmed, M.; Martis, C.; Zuber, D.; Phetsinorath, D.; Gao, F.; et al. Calculation of the GHG emissions of a European research project on electrified vehicles. In Proceedings of the 2021 IEEE Vehicle Power and Propulsion Conference (VPPC), Gijon, Spain, 25–28 October 2021; pp. 1–5. [CrossRef]
2. Jyothi, R.K.; Thenepalli, T.; Ahn, J.W.; Parhi, P.K.; Chung, K.W.; Lee, J.Y. Review of rare earth elements recovery from secondary resources for clean energy technologies: Grand opportunities to create wealth from waste. *J. Clean. Prod.* **2020**, *267*, 122048. [CrossRef]
3. Maask, V.; Agabus, H.; Tiismus, H.; Astapov, V.; Ahmadiahangar, R.; Korõtko, T.; Rosin, A. Exploring the Landscape of End User Energy Flexibility: A Systematic Review of Technologies, Challenges, and Opportunities. *IEEE Access* **2025**, *13*, 146579–146602. [CrossRef]
4. Dutta, T.; Kim, K.-H.; Uchimiya, M.; Kwon, E.E.; Jeon, B.-H.; Deep, A.; Yun, S.-T. Global demand for rare earth resources and strategies for green mining. *Environ. Res.* **2016**, *150*, 182–190. [CrossRef] [PubMed]
5. Shuai, J.; Zhao, Y.; Shuai, C.; Wang, J.; Yi, T.; Cheng, J. Assessing the international co-opetition dynamics of rare earth resources between China, USA, Japan and the EU: An ecological niche approach. *Resour. Policy* **2023**, *82*, 103446. [CrossRef]
6. Ramesh, P.; Lenin, N.C. High Power Density Electrical Machines for Electric Vehicles—Comprehensive Review Based on Material Technology. *IEEE Trans. Magn.* **2019**, *55*, 1–21. [CrossRef]
7. Palangar, M.F.; Soong, W.L. Future Electrical Machine Materials: Possibilities, Opportunities and Challenges. In Proceedings of the 2022 IEEE Energy Conversion Congress and Exposition (ECCE), Detroit, MI, USA, 9–13 October 2022; pp. 1–7. [CrossRef]
8. Bobba, S.; Eynard, U.; Maury, T.; Ardente, F.; Blengini, G.A.; Mathieux, F. Circular Input Rate: Novel indicator to assess circularity performances of materials in a sector—Application to rare earth elements in e-vehicles motors. *Resour. Conserv. Recycl.* **2023**, *197*, 107037. [CrossRef]
9. Santhosh Kumar, R.; Rashmi; Sundara Rajan, J. Recent Advances in Nanocomposite Soft Magnetic Materials: A Review. In Proceedings of the 2022 IEEE International Conference on Nanoelectronics, Nanophotonics, Nanomaterials, Nanobioscience & Nanotechnology (5NANO), Kottayam, India, 28–29 April 2022; pp. 1–6. [CrossRef]
10. Gao, K.; Zou, M.; Ma, B.; Wang, S. Composite magnet solution for high performance green drive. *J. Magn. Magn. Mater.* **2023**, *568*, 170250. [CrossRef]
11. van Nielen, S.S.; Sprecher, B.; Verhagen, T.J.; Kleijn, R. Towards neodymium recycling: Analysis of the availability and recyclability of European waste flows. *J. Clean. Prod.* **2023**, *394*, 136252. [CrossRef]
12. Kontos, S.; Ibrayeva, A.; Leijon, J.; Mörée, G.; Frost, A.E.; Schönström, L.; Gunnarsson, K.; Svedlindh, P.; Leijon, M.; Eriksson, S. An Overview of MnAl Permanent Magnets with a Study on Their Potential in Electrical Machines. *Energies* **2020**, *13*, 5549. [CrossRef]
13. Shin, D.-W.; Kim, D.-S.; Madavali, B.; Kim, D.-H.; Kim, J.-G.; Lee, C.-H.; Challapalli, S.; Hong, S.-J. Densification mechanism and its effect on the magnetic properties of Nd-Fe-B bonded magnets through the new high-energy compaction method. *J. Magn. Magn. Mater.* **2019**, *482*, 280–286. [CrossRef]
14. Zakotnik, M.; Harris, I.R.; Williams, A.J. Multiple recycling of NdFeB-type sintered magnets. *J. Alloys Compd.* **2009**, *469*, 314–321. [CrossRef]
15. Pošković, E.; Franchini, F.; Ceroni, M.; Innocenti, C.; Ferraris, L.; Sangregorio, C.; Caneschi, A.; Actis Grande, M. Study of an Impact Mill-Based Mechanical Method for NdFeB Magnet Recycling. *Metals* **2023**, *13*, 1103. [CrossRef]
16. Tsunata, R.; Takemoto, M.; Ogasawara, S.; Saito, T.; Ueno, T. SMC Development Guidelines for Axial Flux PM Machines Employing Coreless Rotor Structure for Enhancing Efficiency Based on Experimental Results. *IEEE Trans. Ind. Appl.* **2022**, *58*, 3470–3485. [CrossRef]
17. Pošković, E.; Franchini, F.; Fracchia, E.; Vaschetto, S.; Ferraris, L.; Tenconi, A. The Effect of Magnetization on the Production Process of Soft Magnetic Composite Stators of Axial Flux Motors. *IEEE Access* **2025**, *13*, 18983–18993. [CrossRef]
18. Périgo, E.A.; Weidenfeller, B.; Kollár, P.; Füzer, J. Past, present and future of soft magnetic composites. *Appl. Phys. Rev.* **2018**, *5*, 031301. [CrossRef]
19. Muthusamy, M.; Abdel-Mageed, B.S.; Bernier, F.; Lamarre, J.-M.; Grenier, S.; Pillay, P. Impact of Soft Magnetic Composite Materials for Traction Applications. *IEEE Trans. Ind. Appl.* **2025**, *61*, 3737–3752. [CrossRef]

20. Selema, A.; Beretta, M.; Van Coppenolle, M.; Tiismus, H.; Kallaste, A.; Ibrahim, M.N.; Rombouts, M.; Vleugels, J.; Kestens, L.A.; Sergeant, P. Evaluation of 3D-Printed Magnetic Materials For Additively-Manufactured Electrical Machines. *J. Magn. Magn. Mater.* **2023**, *569*, 170426. [CrossRef]
21. Manko, R.; Dmytro, R.; Vukotić, M.; Rupnik, U.; Miljavec, D.; Čorović, S. A Review of Manufacturing Technologies of Soft Magnetic Composites for Electric Machines. In Proceedings of the 2023 IEEE 5th International Conference on Modern Electrical and Energy System (MEES), Kremenchuk, Ukraine, 27–30 September 2023; pp. 1–4. [CrossRef]
22. Hsiang, H.-I.; Fan, L.-F.; Hung, J.-J. Phosphoric acid addition effect on the microstructure and magnetic properties of iron-based soft magnetic composites. *J. Magn. Magn. Mater.* **2018**, *447*, 1–8. [CrossRef]
23. Lee, S.; Choi, M.; Kim, J. Magnetic Properties of Pure Iron Soft Magnetic Composites Coated by Manganese Phosphates. *IEEE Trans. Magn.* **2017**, *53*, 2003304. [CrossRef]
24. Taghvaei, A.H.; Shokrollahi, H.; Janghorban, K. Properties of iron-based soft magnetic composite with iron phosphate–silane insulation coating. *J. Alloys Compd.* **2009**, *481*, 681–686. [CrossRef]
25. Dias, M.M.; Mozetic, H.J.; Barboza, J.S.; Martins, R.M.; Pelegrini, L.; Schaeffer, L. Influence of resin type and content on electrical and magnetic properties of soft magnetic composites (SMCs). *Powder Technol.* **2013**, *237*, 213–220. [CrossRef]
26. Pošković, E.; Ferraris, L.; Franchini, F.; Actis Grande, M. The effect of particle size on the core losses of soft magnetic composites. *AIP Adv.* **2019**, *9*, 035224. [CrossRef]
27. Streckova, M.; Bures, R.; Faberova, M.; Medvecky, L.; Fuzer, J.; Kollar, P. A comparison of soft magnetic composites designed from different ferromagnetic powders and phenolic resins. *Chin. J. Chem. Eng.* **2015**, *23*, 736–743. [CrossRef]
28. Birčáková, Z.; Füzer, J.; Kollár, P.; Streckova, M.; Szabó, J.; Bureš, R.; Fáberová, M. Magnetic properties of Fe-based soft magnetic composite with insulation coating by resin bonded Ni-Zn ferrite nanofibres. *J. Magn. Magn. Mater.* **2019**, *485*, 1–7. [CrossRef]
29. Luo, Z.; Fan, X.; Hu, W.; Luo, F.; Wang, J.; Wu, Z.; Liu, X.; Li, G.; Li, Y. Formation mechanism and enhanced magnetic properties of Fe–Si/Fe_2SiO_4 soft magnetic composites transformed from Fe-6.5 wt%Si/α-Fe_2O_3 core-shell composites. *J. Alloys Compd.* **2020**, *817*, 152803. [CrossRef]
30. Meng, B.; Yang, B.; Zhang, X.; Zhou, B.; Li, X.; Yu, R. Combinatorial surface coating and greatly-improved soft magnetic performance of Fe/Fe_3O_4/resin composites. *Mater. Chem. Phys.* **2020**, *242*, 122478. [CrossRef]
31. Wang, M.; Zan, Z.; Deng, N.; Zhao, Z. Preparation of pure iron/Ni–Zn ferrite high strength soft magnetic composite by spark plasma sintering. *J. Magn. Magn. Mater.* **2014**, *361*, 166–169. [CrossRef]
32. Peng, Y.; Yi, Y.; Li, L.; Ai, H.; Wang, X.; Chen, L. Fe-based soft magnetic composites coated with NiZn ferrite prepared by a co-precipitation method. *J. Magn. Magn. Mater.* **2017**, *428*, 148–153. [CrossRef]
33. Rudeichuk, T.; Olekšáková, D.; Maciaszek, R.; Matysiak, W.; Kollár, P. Exploring the Impact of Different Milling Parameters of Fe/SiO_2 Composites on Their Structural and Magnetic Properties. *Materials* **2024**, *17*, 862. [CrossRef] [PubMed]
34. Liu, L.; Yue, Q.; Li, G.; Xu, K.; Wang, J.; Wu, Z.; Fan, X. Influence of SiO_2 insulation layers thickness distribution on magnetic behaviors of Fe-Si@SiO_2 soft magnetic composites. *J. Phys. Chem. Solids* **2019**, *132*, 76–82. [CrossRef]
35. Li, W.; Zhang, J.; Li, M.; Ying, Y.; Yu, J.; Zheng, J.; Qiao, L.; Li, J.; Che, S. Analysis of Loss Mechanisms Due to Eddy Currents and Hysteresis in Two-Phase Amorphous Hybrid Soft Magnetic Composites. *IEEE Trans. Magn.* **2025**, *61*, 2000207. [CrossRef]
36. Wu, Z.Y.; Jiang, Z.; Fan, X.A.; Zhou, L.J.; Wang, W.L.; Xu, K. Facile synthesis of Fe-6.5wt%Si/SiO_2 soft magnetic composites as an efficient soft magnetic composite material at medium and high frequencies. *J. Alloys Compd.* **2018**, *742*, 90–98. [CrossRef]
37. Füzer, J.; Vovk, S.; Dobák, S.; Kollár, P.; Bureš, R.; Fáberová, M. The effect of temperature on the magnetic properties of Fe/SiO_2/ferrite soft magnetic composites. In Proceedings of the 2023 IEEE International Magnetic Conference—Short Papers (INTERMAG Short Papers), Sendai, Japan, 15–19 May 2023; pp. 1–2. [CrossRef]
38. Fan, X.A.; Wu, Z.Y.; Li, G.Q.; Wang, J.; Xiang, Z.D.; Gan, Z.H. High resistivity and low core loss of intergranular insulated Fe–6.5 wt.% Si/SiO_2 composite compacts. *Mater. Des.* **2016**, *89*, 1251–1258. [CrossRef]
39. Tkáč, M.; Kollár, P.; Olekšáková, D.; Maciaszek, R.; Fáberová, M.; Bureš, R. Influence of Interparticle Electrical Insulators on the Magnetic Permeability of NiFeMo-Based Soft Magnetic Composites. In Proceedings of the IEEE INTERMAG Short Papers, Manchester, UK, 13–17 April 2026; pp. 1–2. [CrossRef]
40. Li, H.; Lu, Z.; Yu, S.; Zhao, M.; Liu, Z.; Li, Z.; Rong, H.; Zhang, X. High Effective Permeability and Low Power Loss of FeSiAl/Al_2O_3/ZnO SMC for High Frequency Application. *Adv. Funct. Mater.* **2024**, *34*, 2403515. [CrossRef]
41. Pošković, E.; Franchini, F.; Actis Grande, M.; Ferraris, L.; Carosio, F.; Tenconi, A. A new approach in the implementation of insulating layers in soft magnetic composite materials. *J. Magn. Magn. Mater.* **2024**, *597*, 171984. [CrossRef]
42. Pošković, E.; Carosio, F.; Ferraris, L.; Franchini, F.; Actis Grande, M. Process for the Production of Nano-Coated Ferromagnetic Materials. PCT Patent No. WO/2023/067471, 27 April 2023.
43. *IEC 60404-3*; Magnetic Materials—Part 3: Methods of Measurement of the Magnetic Properties of Electrical Steel Strip and Sheet by Means of a Single Sheet Tester. Edition 3.0; International Electrotechnical Commission (IEC): Geneva, Switzerland, 2022.

44. *IEC 60404-6*; Magnetic Materials—Part 6: Methods of Measurement of the Magnetic Properties of Magnetically Soft Metallic and Powder Materials at Frequencies in the Range 20 Hz to 100 kHz by the Use of ring Specimens. Edition 3.1; International Electrotechnical Commission (IEC): Geneva, Switzerland, 2021.
45. Pošković, E.; Franchini, F.; Ferraris, L.; Carosio, F.; Actis Grande, M. Rapid Characterization Method for SMC Materials for a Preliminary Selection. *Appl. Sci.* **2021**, *11*, 2133. [CrossRef]
46. Appino, C.; Ferrara, E.; Fiorillo, F.; Rocchino, L.; Ragusa, C.; Sievert, J.; Belgrand, T.; Wang, C.; Denke, P.; Siebert, S.; et al. International comparison on SST and Epstein measurements in grain-oriented Fe-Si sheet steel. *Int. J. Appl. Electromagn. Mech.* **2015**, *48*, 123–133. [CrossRef]
47. Grenda, K.; Idström, A.; Evenäs, L.; Persson, M.; Holmberg, K.; Bordes, R. An analytical approach to elucidate the architecture of polyethyleneimines. *J. Appl. Polym. Sci.* **2022**, *139*, e51657. [CrossRef]
48. Socrates, G. Infrared and Raman Characteristic Group Frequencies. In *Tables and Charts*, 3rd ed.; Wiley: Hoboken, NJ, USA, 2001.
49. Dong, J.; Ozaki, Y.; Nakashima, K. Infrared, Raman, and near-infrared spectroscopic evidence for the coexistence of various hydrogen-bond forms in poly (acrylic acid). *Macromolecules* **1997**, *30*, 1111–1117. [CrossRef]
50. Choi, J.; Rubner, M.F. Influence of the Degree of Ionization on Weak Polyelectrolyte Multilayer Assembly. *Macromolecules* **2005**, *38*, 116–124. [CrossRef]
51. Petreanu, I.; Niculescu, V.C.; Enache, S.; Iacob, C.; Teodorescu, M. Structural Characterization of Silica and Amino-Silica Nanoparticles by Fourier Transform Infrared (FTIR) and Raman Spectroscopy. *Anal. Lett.* **2023**, *56*, 390–403. [CrossRef]
52. Carosio, F.; Alongi, J.; Malucelli, G. A-Zirconium phosphate-based nanoarchitectures on polyester fabrics through layer-by-layer assembly. *J. Mater. Chem.* **2011**, *21*, 10370–10376. [CrossRef]
53. Ariga, K.; Lvov, Y.; Ichinose, I.; Kunitake, T. Ultrathin films of inorganic materials (SiO_2 nanoparticle, montmorillonite microplate, and molybdenum oxide) prepared by alternate layer-by-layer assembly with organic polyions. *Appl. Clay Sci.* **1999**, *15*, 137–152. [CrossRef]
54. Carosio, F.; Di Blasio, A.; Alongi, J.; Malucelli, G. Layer by layer nanoarchitectures for the surface protection of polycarbonate. *Eur. Polym. J.* **2013**, *49*, 397–404. [CrossRef]

Disclaimer/Publisher's Note: The statements, opinions and data contained in all publications are solely those of the individual author(s) and contributor(s) and not of MDPI and/or the editor(s). MDPI and/or the editor(s) disclaim responsibility for any injury to people or property resulting from any ideas, methods, instructions or products referred to in the content.